TU Delft

Delft University of Technology

Document Version
Final published version

Licence
Dutch Copyright Act (Article 25fa)

Citation (APA)
Li, Q., Mosleh, Y., Zhang, H., Li, W., & Alderliesten, R. C. (2025). In-plane compressive properties of 3D braided jute/epoxy composite honeycombs: Structure-property relationships. *Journal of Reinforced Plastics and Composites*, *45*(5-6), 1211-1229. https://doi.org/10.1177/07316844241312729

Important note
To cite this publication, please use the final published version (if applicable).
Please check the document version above.

Copyright
In case the licence states “Dutch Copyright Act (Article 25fa)”, this publication was made available Green Open Access via the TU Delft Institutional Repository pursuant to Dutch Copyright Act (Article 25fa, the Taverne amendment). This provision does not affect copyright ownership.
Unless copyright is transferred by contract or statute, it remains with the copyright holder.

Sharing and reuse
Other than for strictly personal use, it is not permitted to download, forward or distribute the text or part of it, without the consent of the author(s) and/or copyright holder(s), unless the work is under an open content license such as Creative Commons.

Takedown policy
Please contact us and provide details if you believe this document breaches copyrights.
We will remove access to the work immediately and investigate your claim.

This work is downloaded from Delft University of Technology.

Check for updates

JOURNAL OF REINFORCED PLASTICS & COMPOSITES

Original article

Journal of Reinforced Plastics and Composites
2026, Vol. 45(5-6) 1211–1229
© The Author(s) 2025
Article reuse guidelines:
sagepub.com/journals-permissions
DOI: 10.1177/07316844241312729
journals.sagepub.com/home/jrp
Sage

In-plane compressive properties of 3D braided jute/epoxy composite honeycombs: Structure-property relationships

Qian-qian Li[1,2], Yasmine Mosleh[3], Hong-hua Zhang[4], Wei Li[4,5] and René Alderliesten[6]

Abstract

To achieve the integrity of the honeycomb structure without interlocking or bonding, a 3D braided honeycomb structure was designed and developed using natural fiber (jute) reinforced epoxy resin. To optimize the in-plane compressive performance of 3D braided composite honeycombs, the effects of resin, unit cell opening angle, and joint wall length on the in-plane compressive strength, deformability, stiffness and energy absorption were investigated. Furthermore, a theoretical model was established between braiding parameters, geometric parameters of honeycomb cell structure, and in-plane compressive modulus. It is found that if 3D braided composite honeycombs are designed for high load-bearing capacity, it is necessary to reduce the resin strain to failure, increase free wall columns, align the angle between the free wall with the main loading direction, or load along the braiding direction. If the design objective is to maximize the energy absorption, the number of cell rows must be maximized. This study establishes the relationship between braiding parameters, honeycomb geometric parameters, and the in-plane compression performance of the 3D braided composite honeycomb, providing a reference for its structural design and performance optimization.

Keywords

3D braiding, honeycomb structure, in-plane compression, jute fiber, textile bio-composites

Introduction

Honeycomb structures, as a typical cellular structure, have been widely used in various fields for their excellent structural efficiency and good designability.[1–3] Especially fiber-reinforced composite honeycomb structures have shown enormous development potential.

At present, there are several preparation methods for fiber-reinforced composite honeycomb structures, including hot press molding,[4] VARTM,[5] interlocking,[6] 3D printing,[7] and tailor-folding.[8] Stocchi[4] compared two molds used for manufacturing jute fabric reinforced vinyl ester matrix honeycomb structures and demonstrated that lateral compression molds produced superior honeycomb structures compared to molds with fixed inserts. The application of lateral pressure allowed for thinner walls, better removal of excess resin, and effective expulsion of trapped air bubbles. Antony et al.[9] used a thermal press to fabricate honeycomb core structures from hemp fiber woven fabric/polypropylene (PP). Vitale et al.[5] employed the VARTM process to manufacture jute/polyester composite honeycombs. Song[6] applied interlocking technology to prepare honeycomb structures by processing composite

[1]College of Materials Science and Engineering, State Key Laboratory for Modification of Chemical Fibers and Polymer Materials, Donghua University, Shanghai, China
[2]Innovation Center for Textile Science and Technology, Donghua University, Shanghai, China
[3]Biobased Structure and Materials, Faculty of Civil Engineering and Geosciences, Delft University of Technology, Delft, The Netherlands
[4]College of Textiles, Shanghai Collaborative Innovation Center for High Performance Fiber Composites, Donghua University, Shanghai, China
[5]Engineering Research Center of Technical Textile, Ministry Education, Shanghai, China
[6]Aerospace Structures and Materials, Faculty of Aerospace Engineering, Delft University of Technology, Delft, the Netherlands

Corresponding authors:
Wei Li, College of Textiles, Shanghai Collaborative Innovation Center for High Performance Fiber Composites, Donghua University, Shanghai 201620, China.
Email: liwei@dhu.edu.cn

René Alderliesten, Aerospace Structures and Materials, Faculty of Aerospace Engineering, Delft University of Technology, Kluyverweg 1, 2629 HS Delft, the Netherlands.
Email: R.C.Alderliesten@tudelft.nl

Data Availability Statement included at the end of the article

carbon panels into slotted ribs and then assembling them using adhesive bonding between the slots. Pehlivan and Baykasoğlu[10] introduced a corrugation technique in which carbon fiber reinforced polymer (CFRP) sheets are first shaped into a specific form using corrugated molds, and then the corrugated sheets are glued and stacked to build honeycomb blocks. Andrew et al.[7] utilized 3D printing technology to fabricate discontinuous carbon fiber reinforced polyetheretherketone (PEEK) composite honeycomb structures. Wei et al.[11] proposed a tailor-folding method to fabricate all-CFRP honeycomb sandwich panels, involving cutting, folding, curing and assembling. This method reduces the stress concentration and reinforces the constraints between the adjacent cell walls. The out-of-plane compression,[11] shear,[11] in-plane compression,[12] and bending[13] properties of CFRP honeycomb sandwich panels were studied, and three-dimensional failure mechanism maps were constructed to reveal the inherent relationship between the failure modes and geometric parameters. However, most manufacturing processes involve multiple steps. Therefore, developing an integrated honeycomb structure to avoid delamination and weak joints is crucial. By using textile methods to manufacture honeycomb fabrics, without cutting or splicing, and combined with liquid molding technology, it is possible to achieve composite honeycomb structures with inherent structural integrity and fiber continuity. Especially for 3D textile composites, the interlayer strength and damage tolerance of laminated composites have been significantly improved,[14,15] providing the possibility of achieving the overall molding of complex structural components.

In a previous paper, we analyzed in detail the braiding principle, braiding process, and internal structure of 3D braided honeycomb fabrics.[16] In our other paper, the influence of joint wall length on the in-plane compression performance of 3D braided composite honeycombs was also investigated.[16] However, in addition to the joint wall length, other cell parameters such as opening angle, wall thickness, specimen thickness, and free wall length can all affect the mechanical performance of composite honeycombs.[2,17–19]

Compression is a common load condition in engineering applications.[20] Generally, more attention is paid to the mechanical properties of honeycomb structures under out-of-plane performance.[21–25] However, in practical engineering applications, structural components are not only subjected to out-of-plane loads, and the failure does not always occur in the out-of-plane direction. Under out-of-plane compression load, the cell wall bears stress along the hole, while under in-plane compression load, the cell wall is subjected to tension, compression, or bending.[26,27] The impact of the in-plane compression performance of honeycomb structures on their application cannot be ignored.

To further investigate the factors influencing in-plane compression performance, this paper analyzes the effects of resin toughness (strain to failure) and opening angle on in-plane compression performance perpendicular and parallel to the braiding direction, and studies the effect of joint wall length on in-plane compression performance after changing the resin matrix and opening angle. A theoretical formula for the in-plane compressive modulus of 3D braided composite honeycombs is established through force analysis. The theoretical relationship between the material Young's modulus, braiding parameters, honeycomb geometric parameters, and the "molding factor" with the in-plane compressive modulus is also analyzed.

Materials and methods

Materials

The experimental materials used in this study are listed in Table 1. All materials were commercially available products. The resin properties, as provided in the manufacturer's product manual, are detailed in Table 2. The resin and curing

Table 1. Specifications and the sources of commercially available epoxy resins.

Materials	Specifications	Source
Jute yarn (double strands)	The average diameter is 2 mm The linear density is 461.70 tex × 2	JD.com[28]
Epoxy	SWANCOR 2511-1A resin SWANCOR 2511-1BS curing agent	Shangwei (Tianjin) Wind Power Materials Company Limited[29]
Epoxy	EPIKOTETM resin 04908 EPIKOTETM curing agent 04908	Hexion[30]

Table 2. Properties of utilized epoxy resins.[29,30]

Resin name	Density (g/cm³)	Tensile strength (MPa)	Tensile modulus (MPa)	Tensile strain (%)	Flexural strength (MPa)	Flexural modulus (MPa)
SWANCOR 2511	1.1~1.2	67~80	2700~3500	4.5~8.5	110~140	2800~3600
	Curing: 24 h at room temperature (28°C) +8 h post curing at 70°C					
EPIKOTETM 04908	1.15	74	2900	9.4	112	3100
	Curing: 4 h at 70°C + 6 h post curing at 80°C					

agent are mixed in a 10:3 ratio. The mixture was thoroughly stirred to ensure uniform distribution of the hardener. The resin-hardener mixture was subjected to a degassing process under vacuum to remove any entrapped air bubbles, ensuring the consistency and quality of the composite material.

Sample preparation

3D braided honeycomb fabrics were fabricated by controlling the separation and combination of the braid according to changing the interlaced state of jute yarns on a 3D braiding machine, for details on the braiding process and fabric structure, please refer to our published paper.[16] The 3D braided honeycomb fabric is fixed and filled with polytetrafluoroethylene (PTFE) modules, and then cured and molded using Vacuum Assisted Resin Transfer Molding (VARTM), as shown in Figure 1(a). After curing, demold and remove the PTFE module. Finally, obtain the 3D braided composite honeycombs through cutting and polishing, as shown in Figure 1(b). 3D braided composite honeycombs with different epoxy resin toughness (strain to failure), opening angles, and joint wall lengths are shown in Figure 2. The samples are named as follows: C refers to the samples prepared using SWANCOR 2511 resin, D refers to the samples prepared using EPIKOTETM 04908 resin; 120°/90° refers to the opening angle; X refers to loading perpendicular to the braiding direction, while Y only loads parallel to the braiding direction; 1/2/3 respectively refer to the number of rows of cells along the braiding direction.

Sample parameters

The fiber volume fraction[31,32] is crucial for the analysis and evaluation of fiber-reinforced composites, while the relative density[10,33] is one of the key parameters of porous structures and forms the basis for lightweight design. Investigating the geometric parameters, fiber volume fraction, and relative density of 3D braided honeycomb composites is of significant importance for the structural optimization and subsequent mechanical performance evaluation of 3D braided honeycomb composites.

The geometric parameters of the honeycomb structure are defined in Figure 3. The total number of yarns in all samples is 95. The braiding angle α and pitch length h are controlled as such to be similar in all samples and are 32° and 6.7 mm, respectively. The number of yarn columns for free wall m_1 is 2 and the free wall thickness t is 6.24 ± 0.21 mm. The number of yarn columns for joint wall m_2 is 5. The total number of braiding cycles f for all samples is 24. The number of braiding cycles for free wall f_1 is 2 and the free wall length l_1 of all samples is 21 mm. The height of sample H is 15.37 ± 0.22 mm. The other parameters of the samples are shown in Table 3. It should be noted that due to marginal change in fiber volume fraction (less than 2%). The effect of fiber volume fraction variation on mechanical properties will be marginal.

Compression test setup

The compression tests were conducted by a 250 kN capacity Zwick universal testing machine with computer control and data acquisition systems. Each specimen was placed between two rigid plates attached to the machine. The test was controlled by the top plate moving vertically downward to compress the specimens at a loading rate of 2 mm/min.[34] Further details of the test setup can be found in Figure 4 of our published paper.[19]

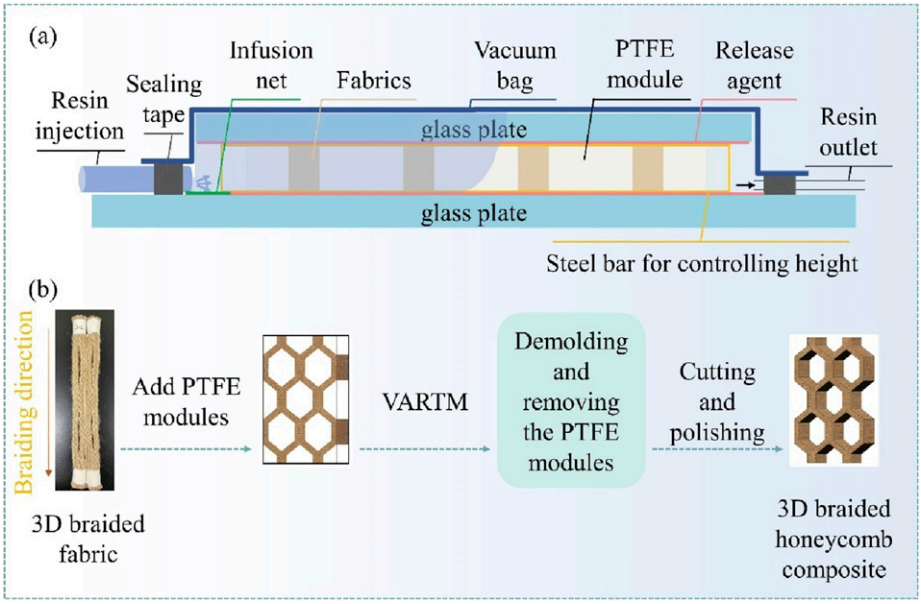

Figure 1. Schematic diagrams of (a) VARTM molding process and (b) manufacturing process of 3D braided composite honeycombs.

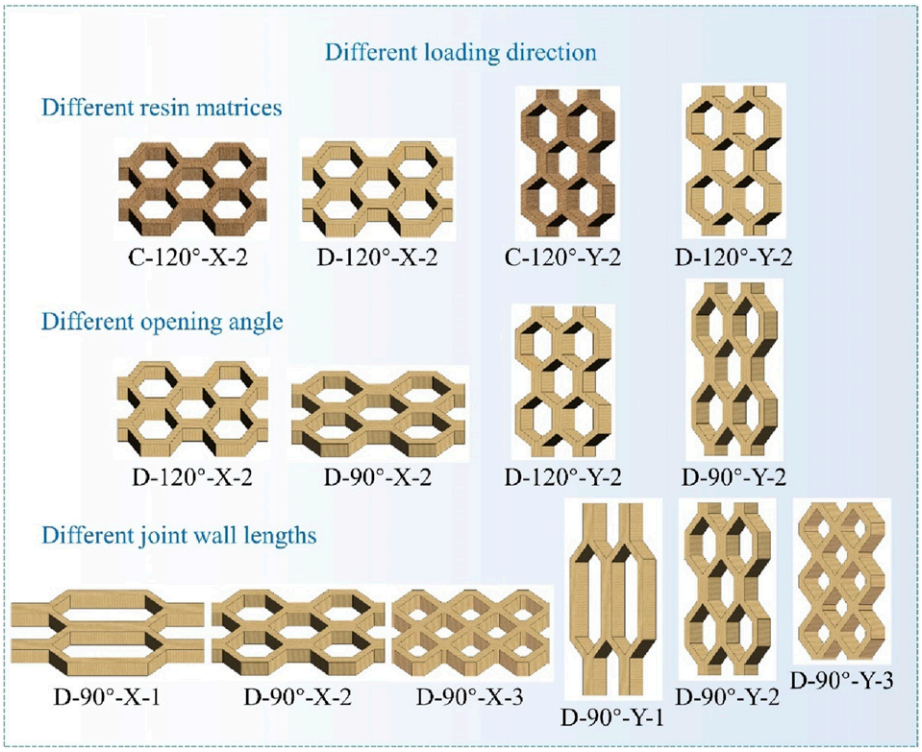

Figure 2. Schematic diagrams of 3D braided composite honeycombs.

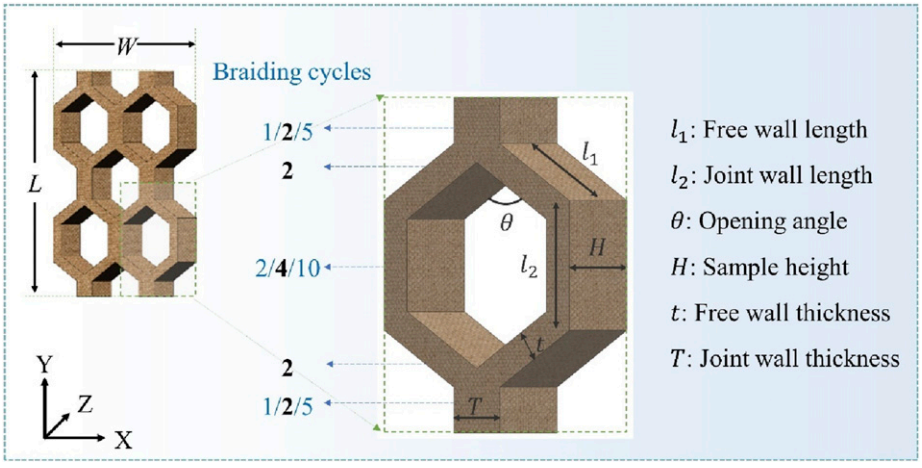

Figure 3. Geometric parameters of 3D braided composite honeycombs (X is vertical to the joint wall; Y is parallel to the joint wall; Z is along the hole direction).

Results and discussions

Effect of resin toughness on in-plane compressive properties of 3D braided composite honeycombs

The difference in load-displacement curves between D-120°-X-2 and C-120°-X-2 is manifested in the load drop or load reduction (BC stage), as shown in Figure 4(a). At this stage, the curve of C-120°-X-2 shows a "cliff-like" drop, while the curve of D-120°-X-2 shows a fluctuating decrease. There are no obvious cracks in C-120°-X-2 before a sudden collapse, as shown in Figure 5(a). Cracks appear sequentially in D-120°-X-2 with tougher resin, but no collapse occurred, as shown in Figure 5(b).

Table 3. The geometrical parameters of the honeycomb samples.

Samples	Width (mm)	Length (mm)	The braiding cycles of joint wall length	Joint wall length (mm)	Fiber volume fraction (%)	Relative density
C-120°-X-2	92.28 ± 0.86	116.20 ± 3.43	4	17	27.48 ± 7.74	0.38 ± 0.04
D-120°-X-2	93.33 ± 1.25	112.33 ± 0.47	4	17	29.92 ± 1.26	0.36 ± 0.01
C-120°-Y-2	92.81 ± 1.09	114.90 ± 1.24	4	17	26.71 ± 7.73	0.37 ± 0.04
D-120°-Y-2	95.67 ± 3.86	117.17 ± 2.32	4	17	27.70 ± 1.99	0.36 ± 0.02
D-90°-X-1	86.38 ± 2.33	148.25 ± 1.30	2	4	27.52 ± 4.63	0.36 ± 0.02
D-90°-X-2	86.83 ± 2.05	133.50 ± 2.55	4	17	28.90 ± 5.97	0.39 ± 0.03
D-90°-X-3	87.27 ± 1.56	130.67 ± 3.30	10	55	26.65 ± 6.40	0.42 ± 0.02
D-90°-Y-1	87.11 ± 3.01	149.25 ± 0.75	2	4	29.24 ± 0.04	0.35 ± 0.02
D-90°-Y-2	87.33 ± 1.52	134.33 ± 1.70	4	17	31.89 ± 2.50	0.37 ± 0.02
D-90°-Y-3	88.00 ± 1.42	129.33 ± 2.05	10	55	28.70 ± 1.20	0.40 ± 0.03

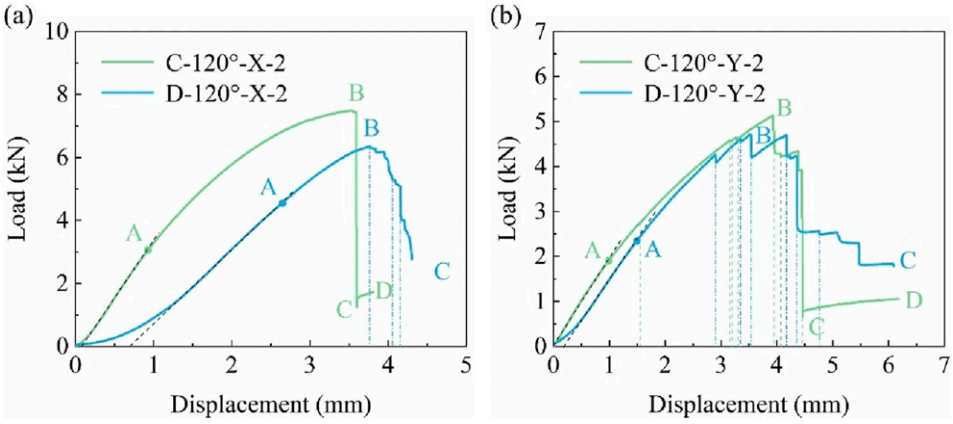

Figure 4. Load-displacement curves of 3D braided composite honeycomb with different resin (a) comparison of curves in *X*-direction and (b) comparison of curves in *Y*-direction.

Compared to C-120°-Y-2, the fluctuation of the curve for D-120°-Y-2 is more pronounced, as shown in Figure 4(b). From the observation of the failure process, the cracks of D-120°-Y-2 and C-120°-Y-2 appear sequentially, but there are more cracks in D-120°-Y-2, as shown in Figure 5(c) and (d), respectively. In summary, using a resin with higher tensile strain to failure (toughness) is beneficial for improving the progressive damage process of the samples and reducing the sudden fracture and thereby collapse of the samples.

The maximum load and compressive strength of 3D braided composite honeycombs with different resin toughness both meet: C-120°-X-2>D-120°-X-2, C-120°-Y-2>D-120°-Y-2, as shown in Figure 6(a). It can be inferred that the use of resin with higher tensile strain to failure reduces the load-bearing capacity of the sample. Compared to the maximum loads of C-120°-X-2 and C-120°-Y-2, the maximum loads of D-120°-X-2 and D-120°-Y-2 are approximately reduced by 30% and 21%, respectively. It can be noted that the resin type has a greater impact on the mechanical properties in the *X* direction. The *Y* direction is both the braiding direction of the sample and the arrangement direction of the yarn, with the yarn playing the main load-bearing role. The *X* direction is perpendicular to the braiding direction, and the resin plays a greater role in this direction than in the *Y* direction. The maximum load and compressive strength also meet the following: C-120°-X-2>C-120°-Y-2, D-120°-X-2>D-120°-Y-2, indicating that for samples with the same free wall columns, the smaller the angle between the free wall and the loading direction, the better the bearing capacity of the sample, as shown in Figure 7.

As observed in Figure 6(b), the displacement and strain at failure in the *X* direction increases, whilst the displacement and strain at failure in the *Y* direction decrease. Compared to C-120°-X-2, the displacement and strain at failure of D-120°-X-2 are increased by approximately 20% and 12%, respectively. The displacement and strain at failure of D-120°-Y-2 are reduced by approximately 11% and 17%, respectively. Changes in the resin have a greater impact on the displacement and strain at failure in the *X* direction.

The compression modulus in both the *X* and *Y* directions decreases, as shown in Figure 6(c). The compressive

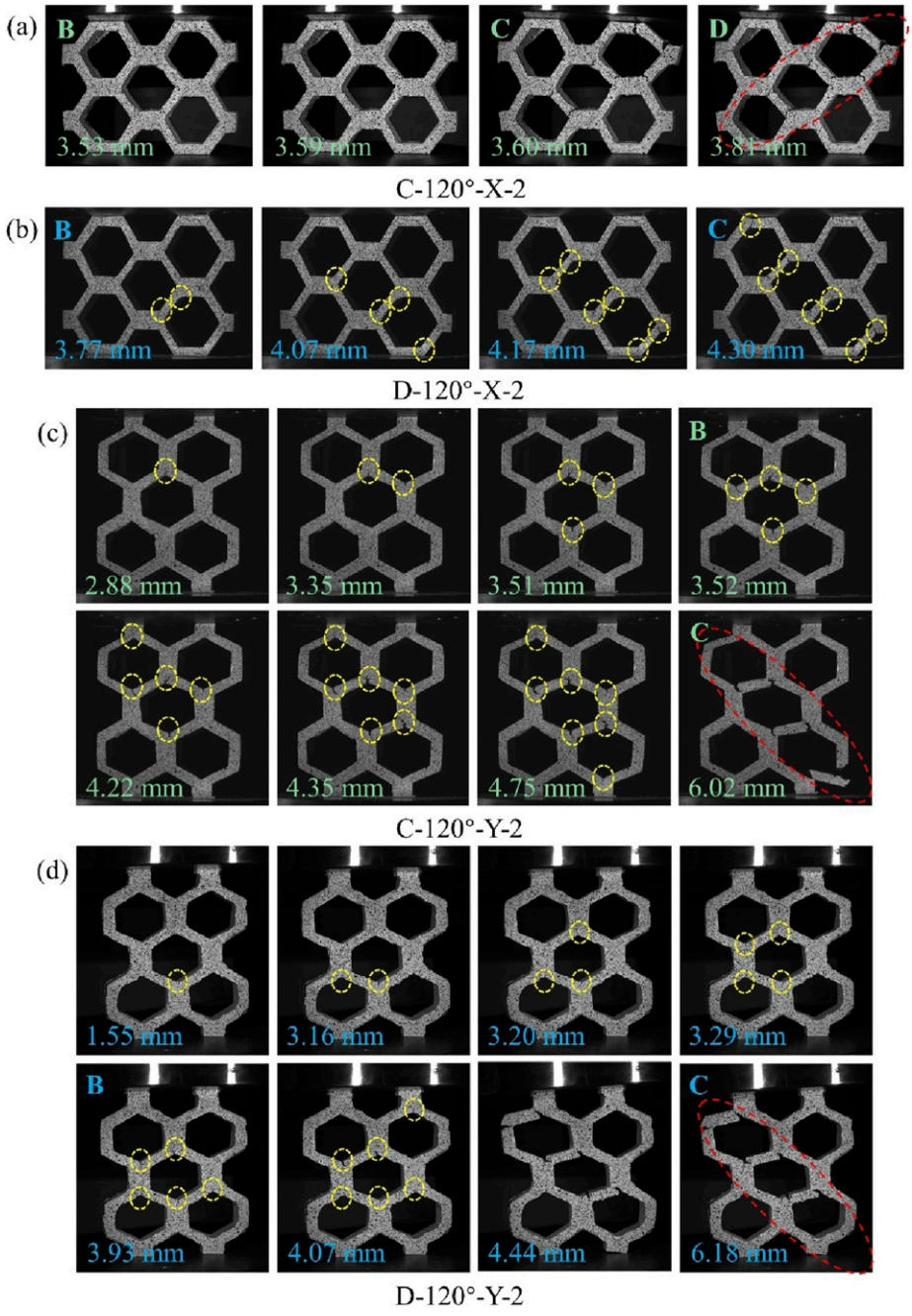

Figure 5. The evolution of failure mechanisms of different samples under compression load (a) C-120°-X-2, (b) D-120°-X-2, (c) C-120°-Y-2 and (d) D-120°-Y-2; illustrating that cracks appear sequentially with increasing displacement, where the yellow dashed box represents the location of crack occurrences.

modulus of D-120°-X-2 and D-120°-Y-2 are approximately 53% and 27% lower than those of C-120°-X-2 and C-120°-Y-2, respectively. This indicates that utilizing a resin with higher tensile strain reduces the in-plane compressive modulus while enhancing deformation capacity. This effect is particularly pronounced in the *X* direction for the in-plane compressive modulus. But the compressive modulus of C-120°-X-2 is greater than that of C-120°-Y-2, while the compressive modulus of D-120°-X-2 is smaller than that of D-120°-Y-2. Due to the greater impact of resin changes on the compression modulus in the *X* direction, the compression modulus in the *X* direction decreases more than in the *Y* direction, resulting in a lower compression modulus for D-120°-X-2 than for D-120°-Y-2.

After using resins with enhanced toughness, the strain energy absorption capacity in both the *X* and *Y* directions

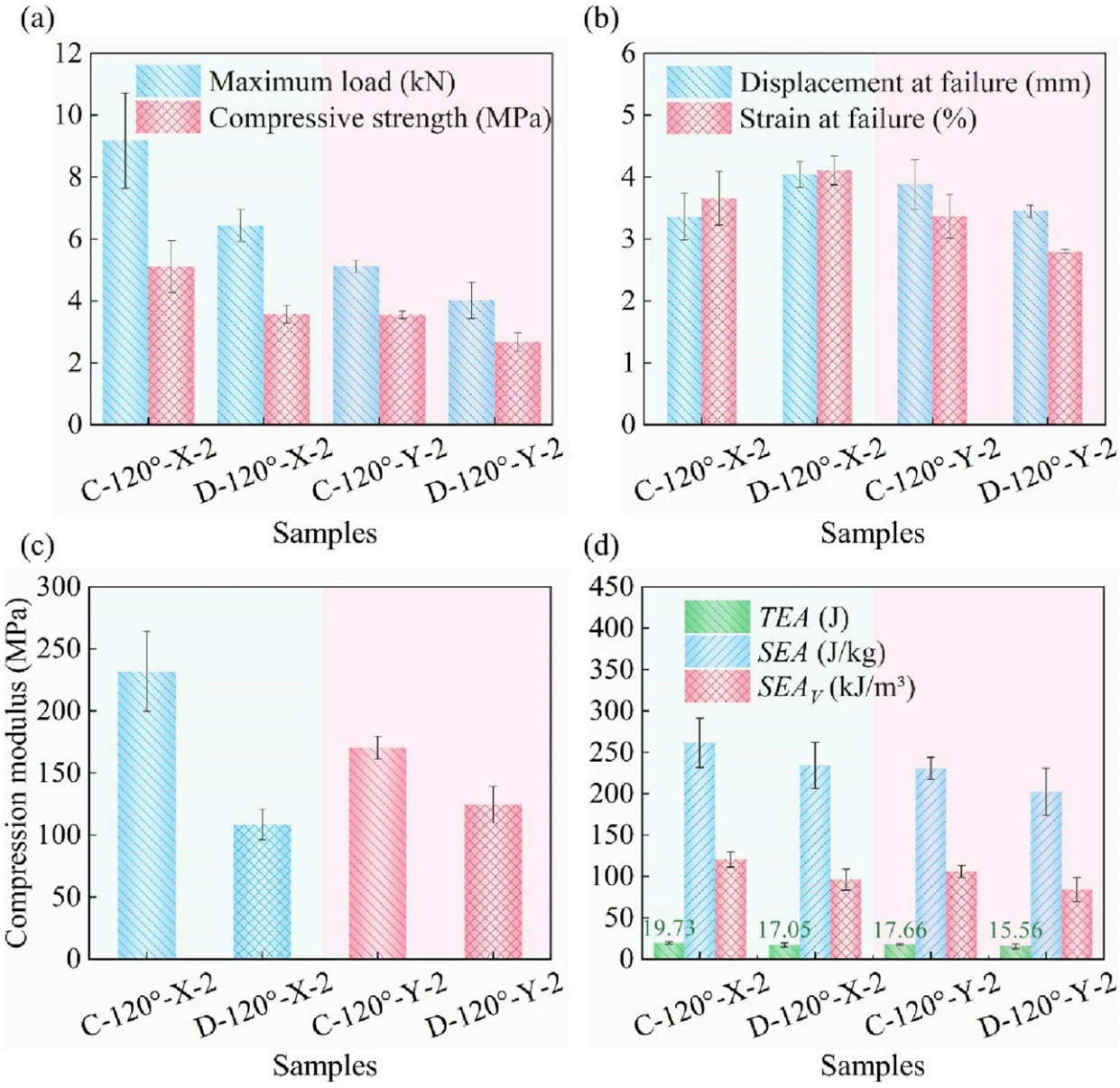

Figure 6. In-plane compression performance of 3D braided composite honeycombs with different resin: (a) bearing capacity, (b) deformation degree, (c) compression modulus, and (d) energy absorption performance.

decreased, as shown in Figure 6(d). Specifically, compared to C-120°-X-2 and C-120°-Y-2, the total energy absorption of D-120°-X-2 and D-120°-Y-2 decreased by approximately 10% and 12%, respectively. Similarly, the volume-specific energy absorption decreased by approximately 20% and 21%. Although using resin with higher tensile strain increases the progressive damage process, it reduces the load-bearing capacity. For *Y* direction loading, it also reduces the displacement and strain at failure. Therefore, changing the resin reduces the energy absorption performance in both the *X* and *Y* directions.

Effect of opening angle on in-plane compressive properties of 3D braided composite honeycombs

The BC stage of the curves for 3D braided composite honeycombs with different opening angles exhibits a fluctuating decline, as depicted in Figure 8(a) and (b) respectively. The failure processes of D-90°-X-2 and D-90°-Y-2 are shown in Figure 9(a) and (b), respectively. The occurrence or propagation of cracks corresponds to the fluctuating descent of the curves.

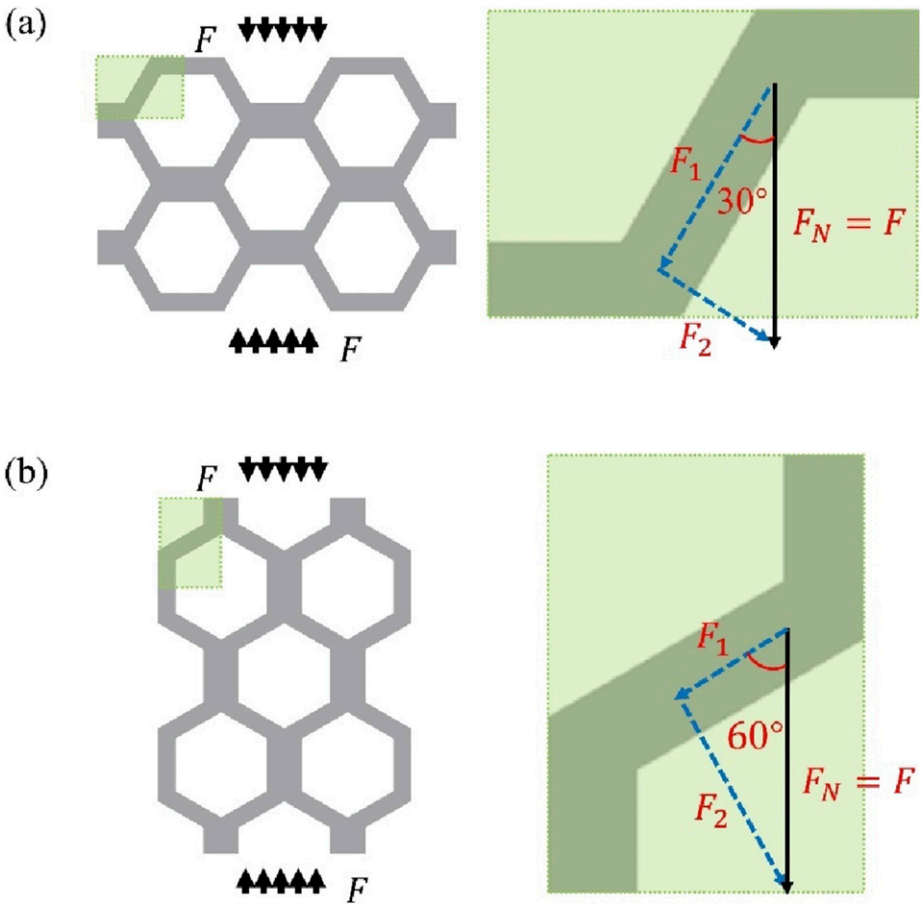

Figure 7. Simplified force analysis of 3D braided composite honeycombs under in-plane compressive load: (a) compressing in the *X* direction and (b) compressing in the *Y* direction.

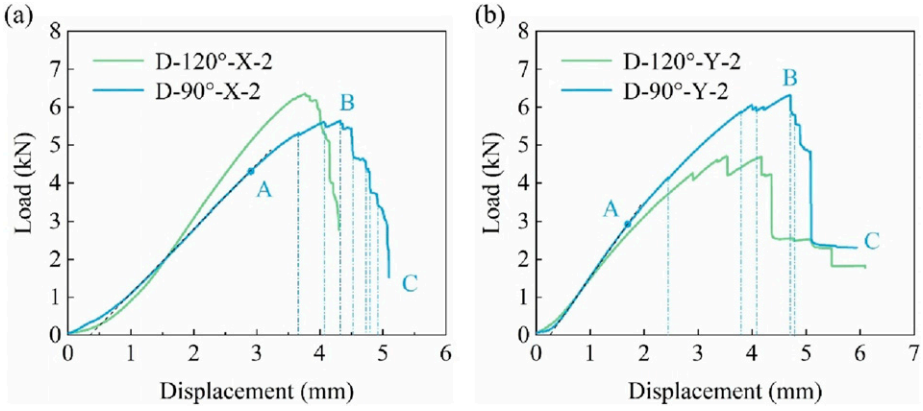

Figure 8. Load-displacement curves of 3D braided composite honeycomb with different opening angle (a) comparison of curves in *X* direction and (b) comparison of curves in *Y* direction.

The comparison of in-plane compression mechanical properties for 3D braided composite honeycombs with different opening angles is shown in Figure 10.

The maximum load and compressive strength in the *X* direction meet the following trend: D-120°-X-2>D-90°-X-2, The maximum load and compressive strength in the *Y* direction follow the order: D-120°-Y-2<D-90°-Y-2, and D-90°-Y-2>D-90°-X-2, as shown in Figure 10(a). For D-120°-X-2, D-90°-X-2, D-120°-Y-2 and D-90°-Y-2, they all have four rows and four columns of free walls, but the angles between

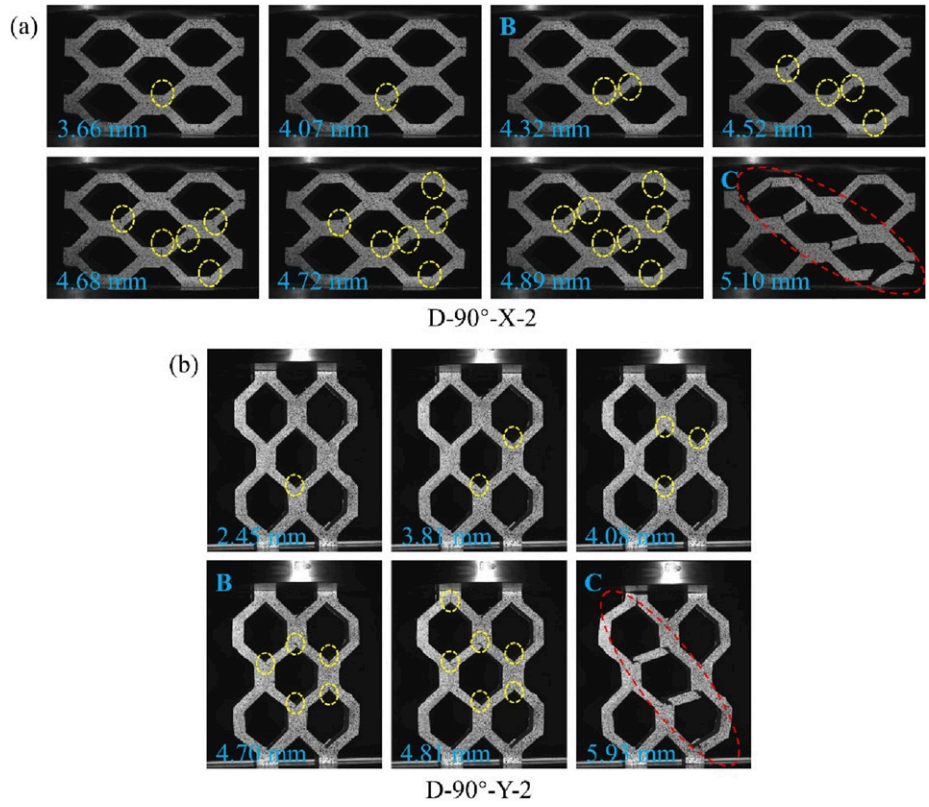

Figure 9. The evolution of failure mechanisms of (a) D-90°-X-2 and (b) D-90°-Y-2; illustrating that cracks appear sequentially with increasing displacement.

their free walls and the joint walls are 30°, 45°, 60°, and 45°, respectively. Figure 7 shows that the smaller the angle between the free wall and the loading direction, the better the load-bearing capacity. Therefore, the bearing capacity follows the order: D-120°-X-2>D-90°-X-2, D-120°-Y-2<D-90°-Y-2. For D-90°-X-2 and D-90°-Y-2, the angle between their free walls and the loading direction is also the same, but the *Y* direction is the braiding direction of the sample, and the yarn plays the main load-bearing role. Therefore, the load-bearing capacity follows the order of D-90°-Y-2>D-90°-X-2. In summary, the bearing capacity follows the order: D-120°-X-2>D-90°-Y-2>D-90°-X-2>D-120°-Y-2.

The displacement and strain at failure follow the order of D-120°-X-2<D-90°-X-2, D-120°-Y-2<D-90°-Y-2, as shown in Figure 10(b). It can be inferred that the larger the opening angle, the smaller the displacement and strain at failure.

The in-plane compressive modulus in the *X* direction is positively correlated with the opening angle. The in-plane compressive modulus in the *Y* direction is negatively correlated with the opening angle, as shown in Figure 10(c). It can be inferred that the larger the opening angle, the stronger the sample's ability to resist in-plane compression deformation in the *X* direction, but the weaker its ability to resist in-plane compression deformation in the *Y* direction.

For total energy absorption, specific energy absorption, and volume-specific energy absorption, all parameters decrease with the opening angle decrease in the *X* direction. Conversely, they increase as the opening angle decreases in the *Y* direction, as illustrated in Figure 10(d).

Effect of joint wall length on in-plane compressive properties of 3D braided composite honeycombs

Samples with an opening angle of 90° and different joint wall lengths were prepared to verify that the effect of joint wall lengths on its in-plane compressive performance is consistent with the specimen with an opening angle of 120°.

The representative in-plane compression curves in the *X* and *Y* directions of 3D braided composite honeycombs with an opening angle of 90° and different joint wall lengths are shown in Figure 11(a) and (b), respectively. The corresponding failure process is shown in Figure 12.

Before the sudden collapse of D-90°-X-1, only one visible crack appeared and extended, and its compression curve showed no significant fluctuations except for a significant linear decrease at B point. As the decrease of

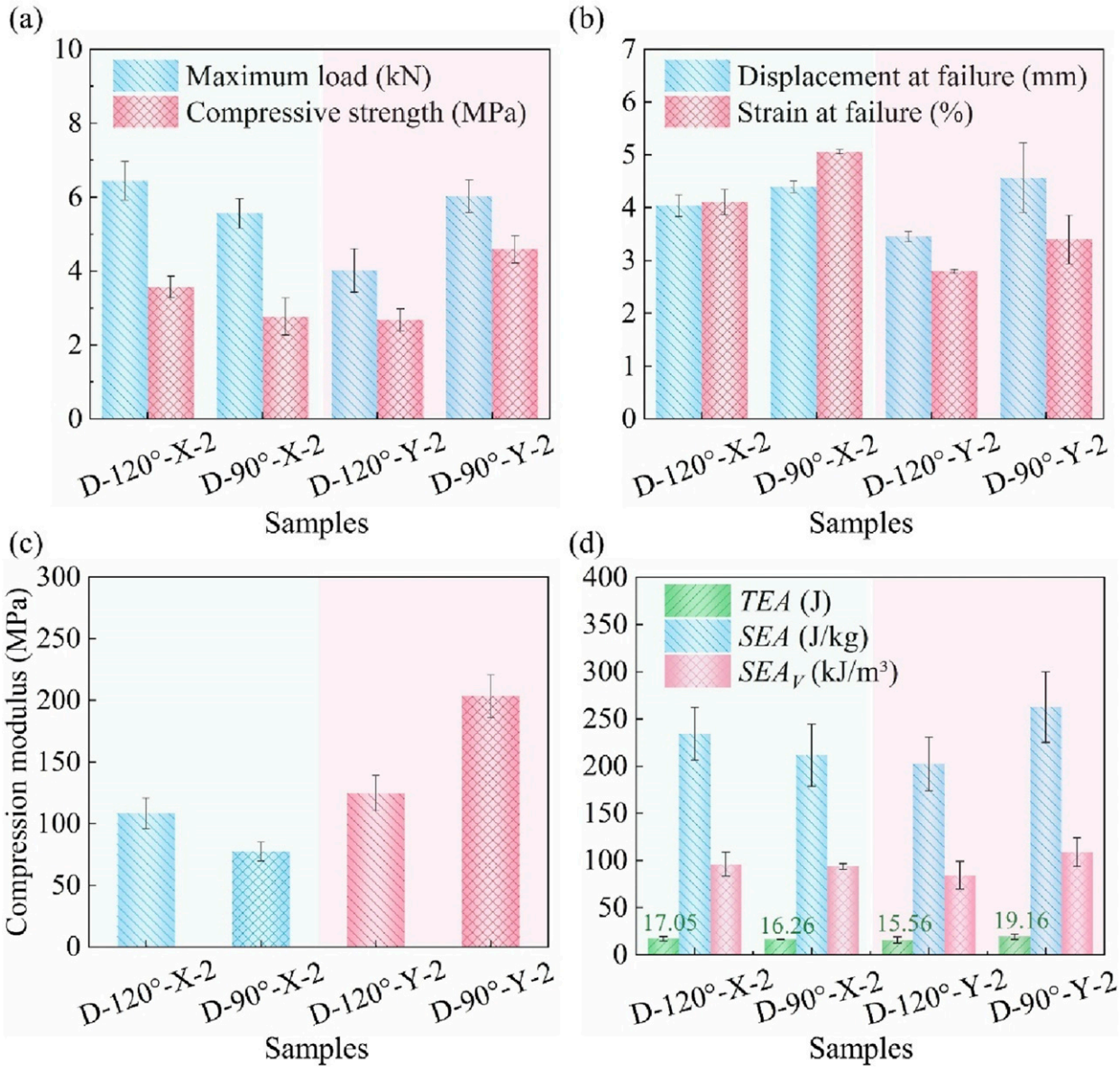

Figure 10. In-plane compression performance of 3D braided composite honeycombs with different opening angles: (a) bearing capacity, (b) deformation degree, (c) compression modulus and (d) energy absorption performance.

joint wall length, the number of cells increases and the number of cracks gradually increases. There are more fluctuations on the compression curves of D-90°-X-2 and D-90°-X-3.

The cracks of D-90°-Y-1 appear sequentially, and due to the sudden and significant expansion of the cracks, the curve shows two consecutive "cliff-like" decreases. The cracks of D-90°-Y-2 increase, with obvious sawtooth shaped fluctuations in the curve. D-90°-Y-3 suddenly collapses when only one crack appears, and the curve has no downward stage.

To explore the influencing factors of maximum load and failure displacement, it is proposed to normalize displacement and load, that is, the maximum load is divided by the number of free wall columns, and the failure displacement is divided by the number of free wall rows.[19]

When the load is along the *X* direction, the maximum load, compressive strength, and compressive modulus increase sequentially with the increase in the number of cell (free wall) columns, that is, D-90°-X-3>D-90°-X-2>D-90°-X-1. The number of free wall rows is the same, and the trend of failure displacement and failure strain is consistent. When the load is along the *Y* direction, the number of free wall rows is the same, and the maximum load and compressive strength tend to be consistent, but

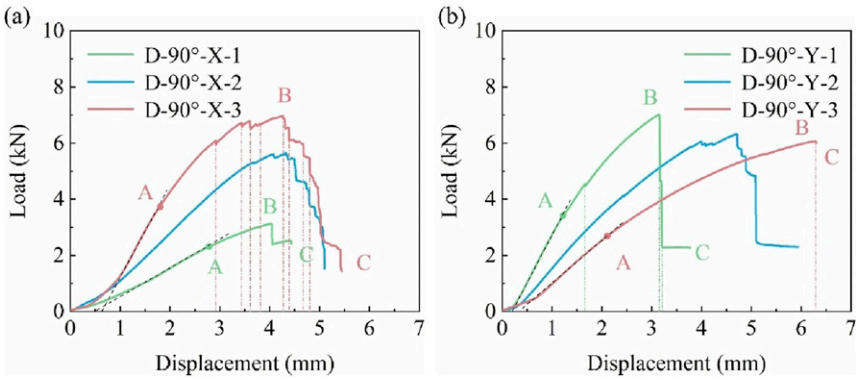

Figure 11. Load-displacement curves of 3D braided composite honeycomb with different joint wall lengths (a) comparison of curves in the *X* direction and (b) comparison of curves in the *Y* direction.

follow the trend: D-90°-Y-1>D-90°-Y-3>D-90°-Y-2. The number of free wall rows increases, the compressive modulus, failure displacement, and failure strain follow as the order: D-90°-Y-3>D-90°-Y-2>D-90°-Y-1. The energy absorption performance increases with the joint wall length reduction and an increase in the number of cells. These in-plane compression mechanical properties for 3D braided composite honeycombs with various joint wall lengths can be found in Figure 13.

From this, it can be seen that the in-plane compressive mechanical properties of D-90° and C-120° follows the same pattern, with changing the resin toughness, cell opening angle, and joint wall length. The bearing capacity is positively correlated with the number of free wall columns. The failure displacement is positively correlated with the number of free wall rows, and the energy absorption performance is positively correlated with the number of unit cells.

Analysis of in-plane compressive modulus of 3D braided composite honeycombs

The in-plane compression modulus is an important parameter for evaluating the mechanical properties of 3D braided composite honeycombs. The influence of different parameters on the in-plane compression modulus has been analyzed through experiments. This part will further establish the relationship between braiding parameters, structural geometric parameters, and in-plane compression modulus through force analysis.

Based on the previous analysis, it can be concluded that the free wall plays the main load-bearing role under in-plane compressive in the *X* direction, and the change in the joint wall length has almost no effect. Therefore, it is assumed that when the specimen is subjected to in-plane compressive stress in the *X* direction σ_x, the deformation of the joint wall can be ignored. As shown in Figure 14, the force F_x acting on the free wall AB can be decomposed into the axial compression force F_a along the free wall and the force F_b that causes the free wall to bend. The free wall AB produces the axial deformation δ_a and the deflection δ_b, respectively, as shown in Supplemental Information 1.

The equivalent strain in the *X* direction is:

$$\varepsilon_x = \frac{\delta_b \cdot \cos\frac{\theta}{2} + \delta_a \cdot \sin\frac{\theta}{2}}{l_1 \cdot \sin\frac{\theta}{2}} = \frac{\sigma_x\left(\cos\frac{\theta}{2} + \frac{l_2}{l_1}\right)\left[\left(\cos\frac{\theta}{2}\right)^2 + \left(\frac{t}{l_1}\right)^2\left(\sin\frac{\theta}{2}\right)^2\right]}{E\left(\frac{t}{l_1}\right)^3 \sin\frac{\theta}{2}} \quad (1)$$

The equivalent strain in the *Y* direction is:

$$\varepsilon_y = \frac{\delta_b \cdot \sin\frac{\theta}{2} + \delta_a \cdot \cos\frac{\theta}{2}}{l_1 \cdot \cos\frac{\theta}{2} + l_2} = \frac{\sigma_x \cdot \sin\frac{\theta}{2} \cdot \cos\frac{\theta}{2} \cdot \left[1 + \left(\frac{t}{l_1}\right)^2\right]}{E\left(\frac{t}{l_1}\right)^3} \quad (2)$$

The in-plane compression modulus of 3D braided composite honeycombs in the *X* direction is

$$E_x = \frac{\sigma_x}{\varepsilon_x} = \frac{\sin\frac{\theta}{2}\left(\frac{t}{l_1}\right)^3 E}{\left(\cos\frac{\theta}{2} + \frac{l_2}{l_1}\right)\left[\left(\cos\frac{\theta}{2}\right)^2 + \left(\frac{t}{l_1}\right)^2\left(\sin\frac{\theta}{2}\right)^2\right]} \quad (3)$$

When the specimen is subjected to in-plane compressive stress in the *Y* direction σ_y, both the free wall and the joint wall deform, as shown in Figure 15. The force F_y acting on the free wall AB can be decomposed into the

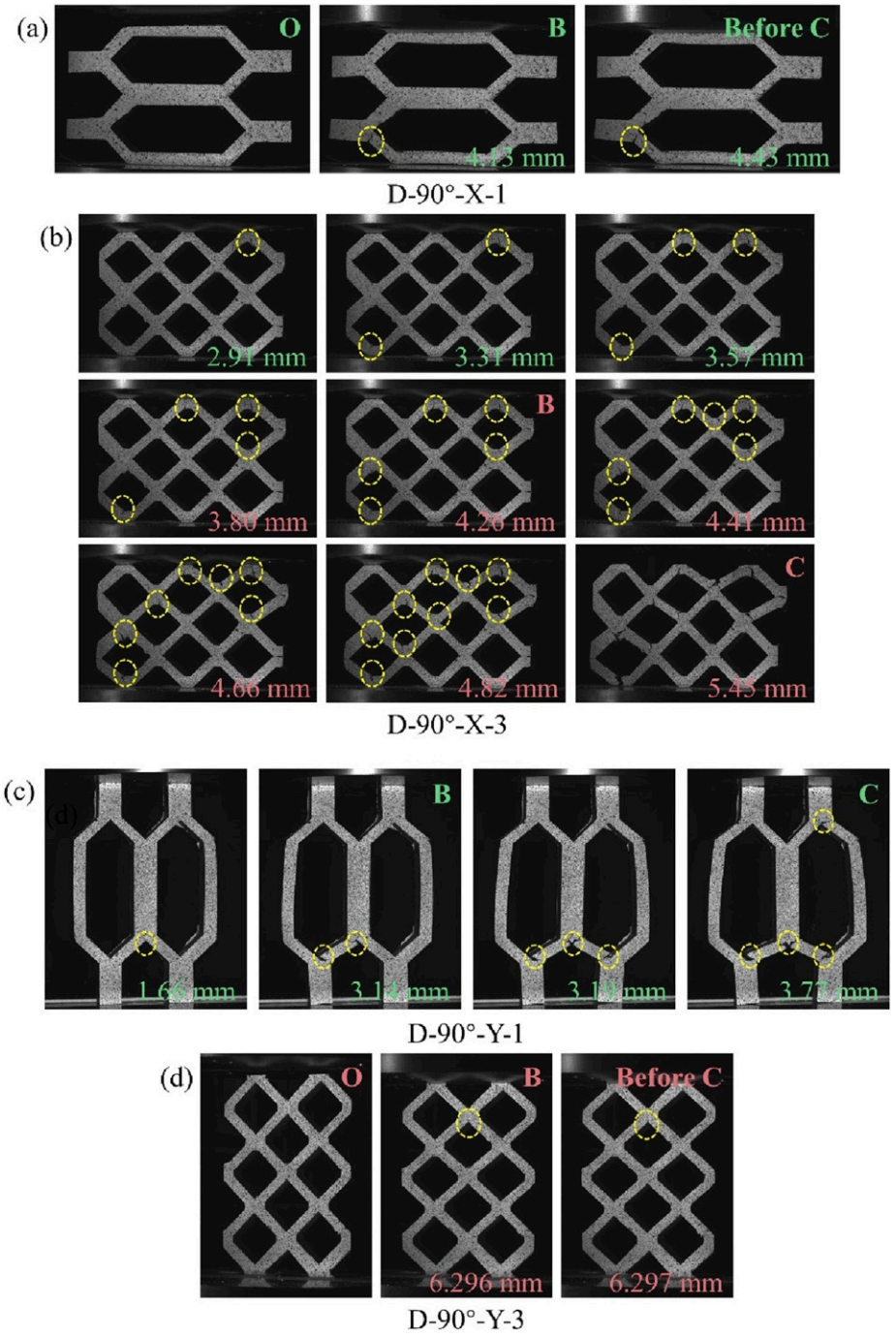

Figure 12. The evolution of failure mechanisms of (a) D-90°-X-1, (b) D-90°-X-3, (c) D-90°-Y-1, and (d) D-90°-Y-3; illustrating that cracks appear sequentially with increasing displacement.

axial compression force F_a along the free wall and the force F_b that causes the free wall to bend. The free wall AB produces the axial deformation δ_a and the deflection δ_b, respectively. The joint wall AC is subjected to a force F_y, resulting in axial deformation δ_c, as shown in Supplemental Information 2.

The equivalent strain in the X direction is:

$$\begin{aligned}\varepsilon_x &= \frac{\delta_b \cdot \cos\frac{\theta}{2} + \delta_a \cdot \sin\frac{\theta}{2}}{l_1 \cdot \sin\frac{\theta}{2}} \\ &= \frac{\sigma_y \cdot \sin\frac{\theta}{2} \cdot \cos\frac{\theta}{2} \cdot \left[\cos\frac{\theta}{2}\left(\frac{t}{l_1}\right)^2 + 1\right]}{E\left(\frac{t}{l_1}\right)^3}\end{aligned} \tag{4}$$

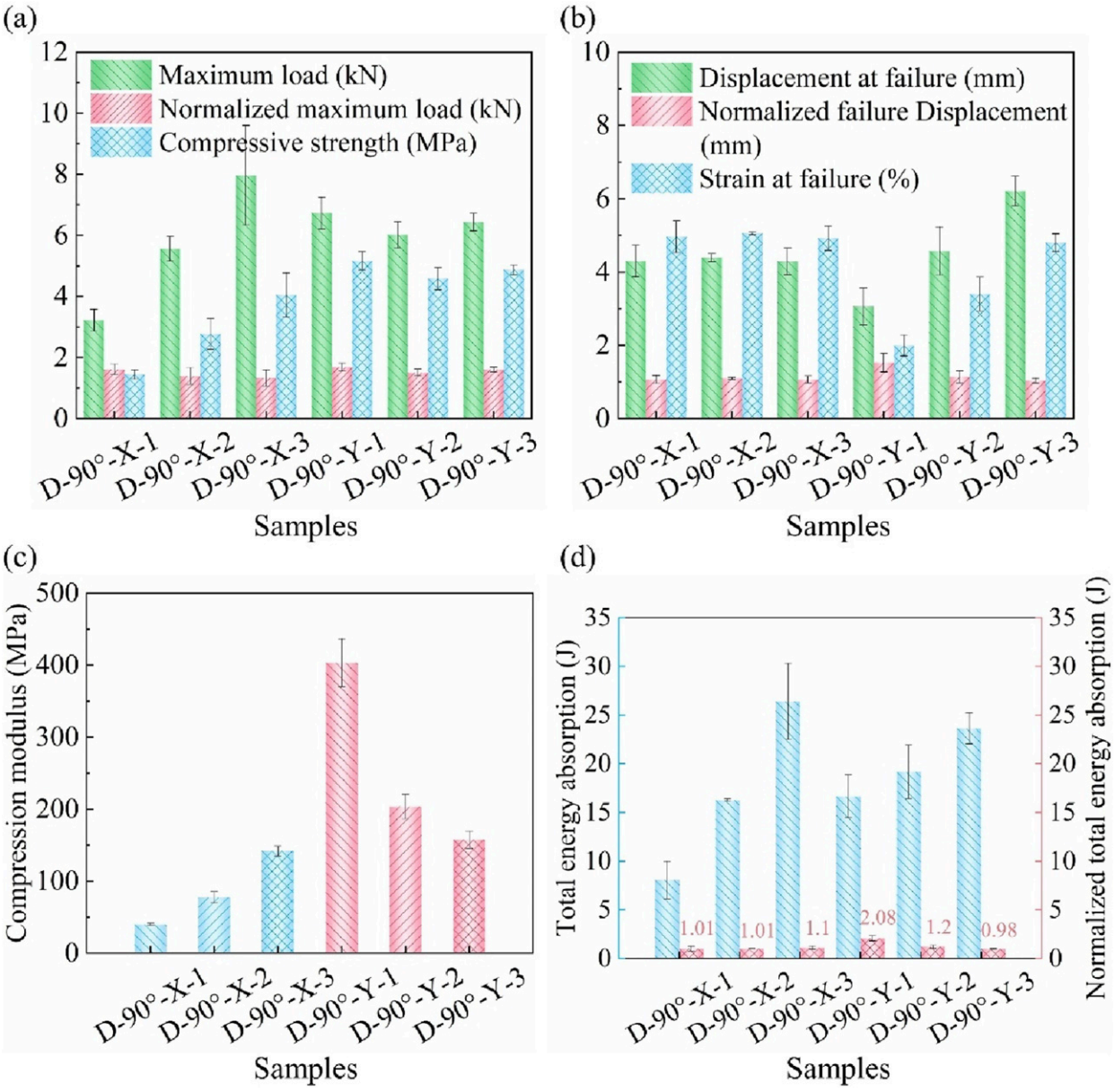

Figure 13. In-plane compression performance of D-90° with different joint wall lengths in different loading directions: (a) bearing capacity, (b) deformation degree, (c) compression modulus, and (d) energy absorption performance.

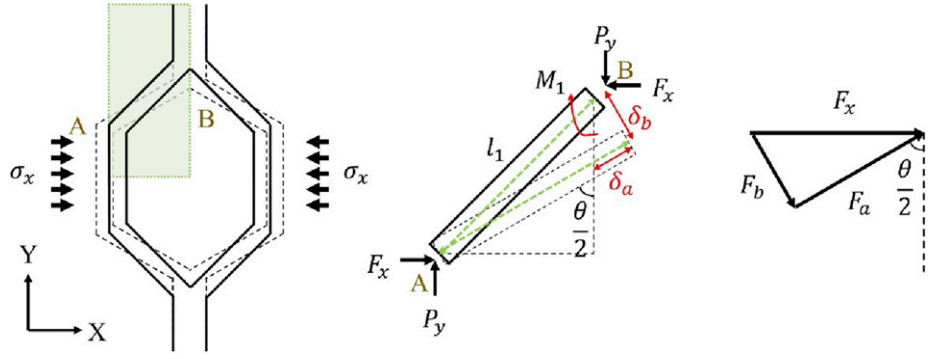

Figure 14. Analysis of deformation and force of honeycomb structures under in-plane compressive loads in *X* direction.

The equivalent strain in the Y direction is:

$$\varepsilon_y = \frac{\sigma_y \cdot \sin\frac{\theta}{2} \cdot \left\{ \left(\sin\frac{\theta}{2}\right)^2 + \left(\frac{t}{l_1}\right)^2 \cdot \left[\left(\cos\frac{\theta}{2}\right)^2 + \frac{l_2}{l_1} \right] \right\}}{E\left(\cos\frac{\theta}{2} + \frac{l_2}{l_1}\right)\left(\frac{t}{l_1}\right)^3} \quad (5)$$

The in-plane compression modulus in the Y direction of 3D braided composite honeycombs is

$$E_y = \frac{\sigma_y}{\varepsilon_y} = \frac{E\left(\cos\frac{\theta}{2} + \frac{l_2}{l_1}\right)\left(\frac{t}{l_1}\right)^3}{\sin\frac{\theta}{2}\left\{ \left(\sin\frac{\theta}{2}\right)^2 + \left(\frac{t}{l_1}\right)^2 \left[\left(\cos\frac{\theta}{2}\right)^2 + \frac{l_2}{l_1} \right] \right\}} \quad (6)$$

According to the relationship between the braiding parameters and the geometric parameters of the honeycomb structure,[16,19] it can be concluded that:

$$\frac{t}{l_1} = \frac{m_1 + \sqrt{2} - 1}{2f_1 + 4r} \cdot \tan\alpha \quad (7)$$

$$\frac{l_2}{l_1} = \frac{f_2 - 2r}{f_1 + 2r} \quad (8)$$

To address inaccuracies resulting from discrepancies between actual and theoretical values of honeycomb geometric parameters, a correction coefficient λ has been introduced. For details, please refer to Supplemental Information 3. The in-plane compressive modulus in the X and Y directions of 3D braided composite honeycombs are as follows:

$$E_x = \frac{\sigma_x}{\varepsilon_x} = \frac{E \cdot \sin\frac{\theta}{2} \cdot \left(\lambda \cdot \frac{m_1+\sqrt{2}-1}{2f_1+2r} \cdot \tan\alpha\right)^3}{\left(\cos\frac{\theta}{2} + \lambda \cdot \frac{f_2-2r}{f_1+r}\right)\left[\left(\cos\frac{\theta}{2}\right)^2 + \left(\lambda \cdot \frac{m_1+\sqrt{2}-1}{2f_1+2r} \cdot \tan\alpha\right)^2 \left(\sin\frac{\theta}{2}\right)^2 \right]} \quad (9)$$

$$E_y = \frac{\sigma_y}{\varepsilon_y} = \frac{E\left(\cos\frac{\theta}{2} + \lambda \cdot \frac{f_2-2r}{f_1+1.5r}\right)\left(\lambda \cdot \frac{m_1+\sqrt{2}-1}{2f_1+3r} \cdot \tan\alpha\right)^3}{\sin\frac{\theta}{2}\left\{ \left(\sin\frac{\theta}{2}\right)^2 + \left(\lambda \cdot \frac{m_1+\sqrt{2}-1}{2f_1+3r} \cdot \tan\alpha\right)^2 \left[\left(\cos\frac{\theta}{2}\right)^2 + \lambda \cdot \frac{f_2-2r}{f_1+1.5r} \right] \right\}} \quad (10)$$

Based on the actual ratio of wall thickness to wall length, as well as the ratio of free wall length to joint wall length, the correction coefficients λ for E_x and E_y are determined to be 1.25 and 1.11, respectively. The theoretical and experimental values of in-plane compression modulus are compared in Table 4, with errors within 15%.

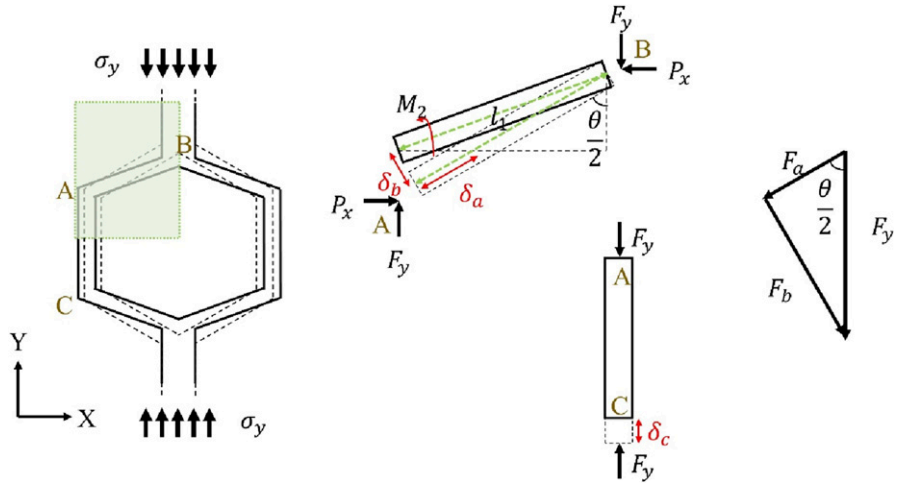

Figure 15. Analysis of deformation and force of honeycomb structures under in-plane compressive loads in Y direction.

Table 4. The theoretical and experimental values of compressive modulus.

Samples	r	f_1	f_2	m_1	α (°)	θ (°)	Theoretical value (MPa)	Experimental value (MPa)	Error (%)
C-120°-X-1	0.66	2	10	2	32	120	92.43	94.62 ± 11.72	2.32
C-120°-X-2	0.66	2	4	2	32	120	230.73	231.87 ± 32.32	0.49
C-120°-X-3	0.66	2	2	2	32	120	460.30	480.05 ± 11.87	4.11
C-120°-Y-1	0.66	2	10	2	32	120	357.61	314.50 ± 5.26	13.71
C-120°-Y-2	0.66	2	4	2	32	120	169.38	170.41 ± 9.09	0.60
C-120°-Y-3	0.66	2	2	2	32	120	93.13	107.44 ± 9.28	13.32

According to equations (9) and (10), it can be seen that the in-plane compressive modulus of 3D braided composite honeycombs is related to E, f_1, f_2, m_1, α, θ and r. The influence of different variables on the in-plane compression modulus is shown in Figure 16.

The in-plane compressive modulus E_x and E_y shows a linear positive correlation with the Young's modulus of the material E, as shown in Figure 16(a). A higher Young's modulus results in a greater in-plane compressive modulus, with Young's modulus having a greater influence on the in-plane compressive modulus in the X direction.

The in-plane compressive modulus in the X direction and Y direction are both negatively correlated with the braiding cycles of the free wall. However, the in-plane compressive modulus in the X direction is negatively correlated with the braiding cycles of the joint wall, whereas the in-plane compressive modulus in the Y direction shows a positive correlation with the braiding cycles of the joint wall. As shown in Figure 16(b), an increase in f_1 results in decreases in both E_x and E_y. Conversely, an increase in f_2 leads to a decrease in E_x and an increase in E_y.

The in-plane compressive modulus in the X direction and Y direction both exhibit a positive correlation with the number of yarn columns in the free wall, as shown in Figure 16(c). As the number of yarn columns in the free wall m_1 increases, both E_x and E_y increase.

The in-plane compressive modulus in the X direction and Y direction both exhibit a positive correlation with the braiding angle α, as illustrated in Figure 16(d). As α increases, both E_x and E_y increase.

The in-plane compressive modulus of 3D braided composite honeycombs in the X direction shows a positive correlation with the opening angle, whereas the in-plane compressive modulus in the Y direction exhibits a negative correlation with the opening angle, as depicted in Figure 16(e). As θ increases, E_x increases while E_y decreases. This explains why the in-plane compressive modulus in Figure 10(c) follows such trends of: D-120°-X-2>D-90°-X-2, and D-120°-Y-2<D-90°-Y-2.

The in-plane compressive modulus in the X direction and Y direction of 3D braided composite honeycombs both exhibit a negative correlation with the "molding factor" r, as shown in Figure 16(f). A larger r results in smaller values of E_x and E_y. As observed, the influence of the "molding factor" r on the in-plane compressive modulus in the Y direction is more significant.

Failure analysis

Whether one changes the resin toughness and cell opening angle, the joint wall length, or loading direction, the crack positions of the 3D braided composite honeycombs show an overall oblique strip shape distribution on the sample, and the sample exhibits "shear-type" failure, as shown in Figure 17. This is consistent with the conclusion obtained by Papka and Kyriakides[35,36] that hexagonal aluminum honeycomb and polycarbonate circular honeycomb collapse in a shear mode under in-plane compressive load. It can be inferred that "shear-type" collapse is a common failure characteristic of honeycomb structures.

The failure positions are all at the intersection of the joint wall and the free wall, which is the "Y-shaped" connection. The main failure types include yarn pull-out, fiber pull-out, fiber breaking, matrix breaking, and fiber-matrix debonding.[19] For detailed information on the fracture surface characteristics, please refer to our published paper.[19] Under the in-plane compression load in the X direction, cracks fracture and expand from the outer side towards the inner side of the "Y-shaped" connection. While under the in-plane compression load in the Y direction, cracks fracture and expand from the inner side towards the outer side of the "Y-shaped" connection. This is because under in-plane compression load, a plastic hinge is formed at the "Y-shaped" connection, as shown in Figure 18. The green circular area represents the intersection area between the joint wall and the free wall.

When the load is along in the X direction, the sample shrinks in the width direction and expands in the length direction. The opening angle tends to shrink inward and decrease. The free wall will rotate inward towards the opening angle. The rotation will also force the joint wall to move to the left, but the joint wall will hinder this deformation. Therefore, the green circular area shows lateral compression. Similarly, rotating the free wall inward will cause the other end of the two free walls to deflect upwards and downwards, respectively, resulting in longitudinal stretching in the green circular area. As shown in Figure 18(a).

When the load is along in the Y direction, the sample shrinks in the length direction and expands in the width direction. The opening angle tends to expand outward and increase. The free wall will rotate towards the outside of the opening angle, and the other end of the two free walls will compress each other. Therefore, the green circular area shows lateral compression. Similarly, the rotation of the free wall to the outside will cause the other end of the two free walls to deflect downwards. The connection between the free wall and the joint wall will drive the joint wall to move downwards, but the joint wall will hinder this deformation. Therefore, the green circular area shows longitudinal stretching. As shown in Figure 18(b).

The above analysis correspond to the description in our previous paper[19] where we concluded: "3D braided composite honeycombs exhibit transverse compressive strain and longitudinal tensile strain at the intersection of the free wall and joint wall under in-plane compressive load."

Regardless of whether the in-plane compressive load is applied in the X or Y direction, there is an angle between the

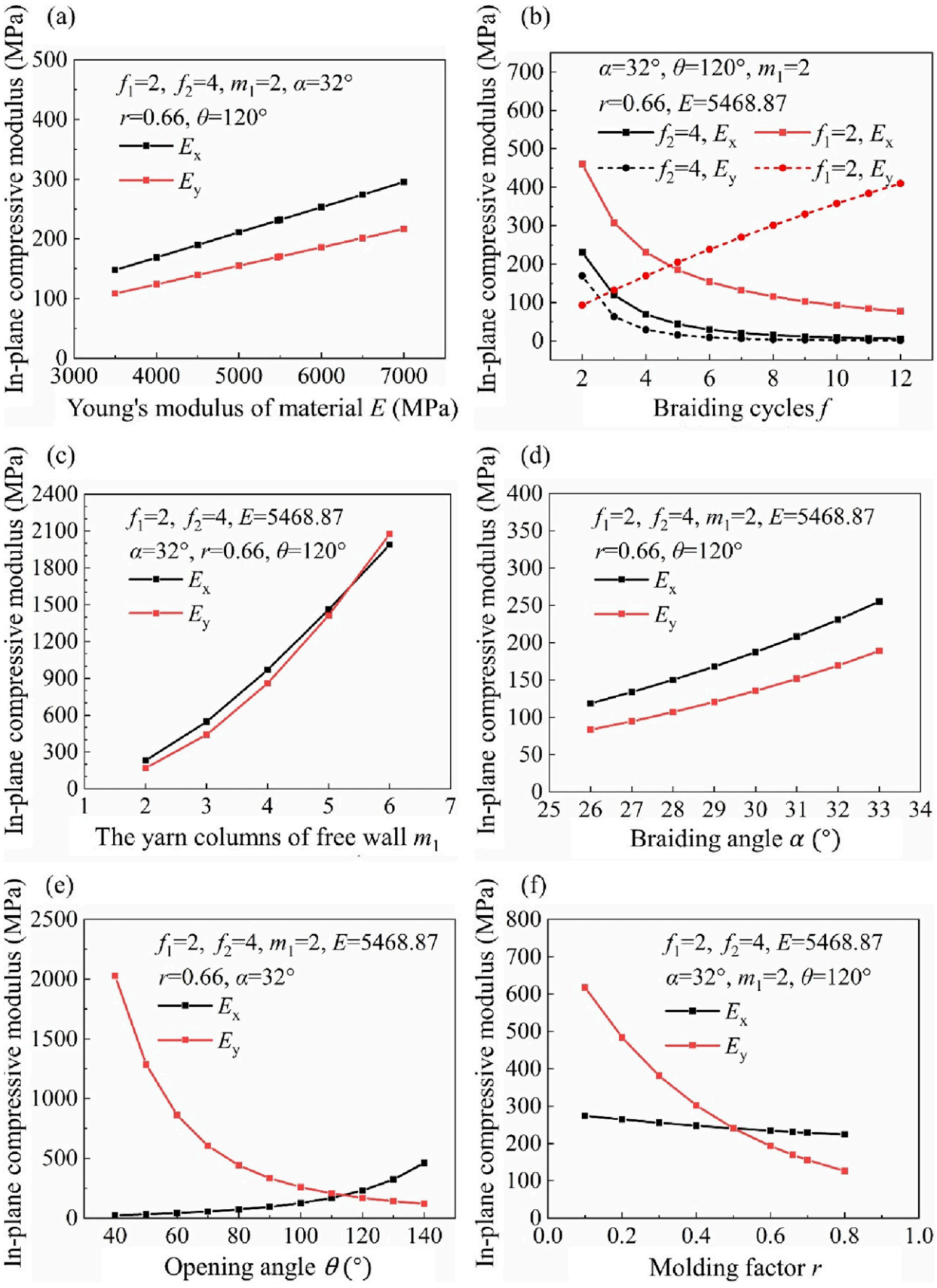

Figure 16. The influence of variables on the in-plane compressive modulus of 3D braided composite honeycombs: (a) Young's modulus of material, (b) braiding cycles, (c) the yarn columns of free wall, (d) braiding angle, (e) opening angle, and (f) "molding factor."

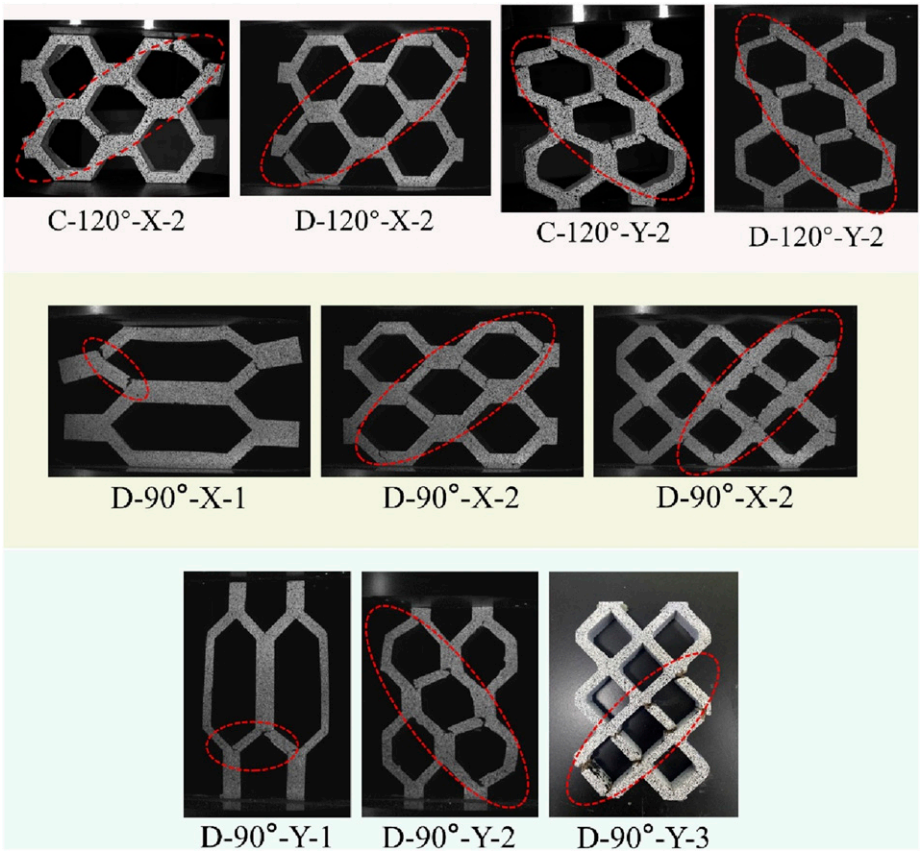

Figure 17. The samples exhibit "shear-type" failure with an inclined strip shape.

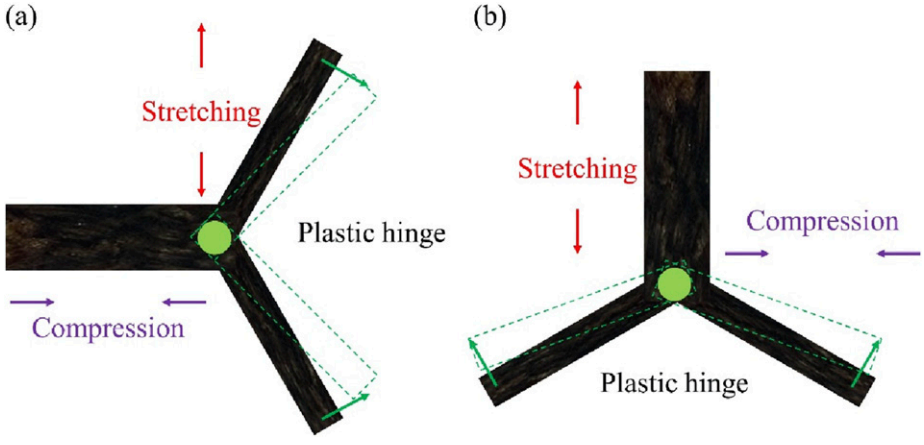

Figure 18. Deformation of plastic hinges (a) in-plane compression in *X* direction and (b) in-plane compression in *Y* direction.

free wall and the loading direction. The free wall is too thick to bend or fold, hence it will bear shear deformation. Once cracks are generated at the intersection of the joint wall and the free wall, the 3D braided composite honeycombs will become unstable and tilt, causing large deformation and crack generation and propagation. Cracks will propagate from single cells to adjacent diagonal cells until cracks penetrate the entire length or width of the specimen, and the specimen will completely collapse. From this, it can be seen that the cracks in the 3D braided composite honeycombs are distributed in an inclined strip shape on the specimen as a whole.

Conclusion

This paper experimentally investigates the effects of resin toughness (strain to failure), loading direction, opening angle, and joint wall length on the in-plane stiffness, strength, deformability and energy absorption capability of 3D braided composite honeycombs, and establishes structure-property relationships. Moreover, a theoretical model to describe the in-plane compressive stiffness of 3D braided composite honeycombs is developed enabling further investigation of influencing material and geometrical parameters on in-plane compressive modulus. Furthermore, damage analysis is carried out and the evolution of failure mechanisms is visualized using camera snapshots. The findings of this study are listed as follows:

(1) Irrespective of resin toughness, loading direction, and geometric parameters such as honeycomb cell opening angle, and joint wall length: the maximum load and deformation to failure increase with the number of free wall columns. Moreover, reducing the cell size (increasing the cell number) improves the energy absorption capacity of the composite honeycombs.
(2) The resin with a higher tensile strain to failure leads to more progressive damage during the failure process, while also reducing the load-bearing capacity and energy absorption capability of the specimens. The change in resin strain to failure has a greater impact on the in-plane compression performance perpendicular to the braiding direction.
(3) The in-plane compressive modulus of the composite honeycombs perpendicular to the braiding direction increases with an increase in Young's modulus of composites, the number of yarn columns in the free wall, the braiding angle, and the opening angle, conversely, it is negatively correlated with the number of braiding cycles in both the free and joint walls and the "filling factor."
Along the braiding direction, the in-plane compressive modulus increases with Young's modulus of composites, the number of braiding cycles in the joint wall, the number of yarn columns in the free wall, and the braiding angle, but is negatively correlated with the number of braiding cycles in the free wall, the opening angle, and the "filling factor."
(4) The 3D braided composite honeycombs exhibit "shear-type" failure, with cracks distributed in an inclined strip shape on the specimen as a whole. The failure positions are all at the "Y-shaped" connection formed by the intersection of the joint wall and the free wall.

This paper offers a detailed analysis of structure-property relationships giving guidelines as to how to optimize the in-plane compression performance of 3D braided composite honeycombs by tailoring their key geometrical parameters. This study provides a valuable theoretical reference for the structural design, performance enhancement, and application development of 3D braided composite honeycombs. Furthermore, natural fibers such as jute offer an environmentally friendly alternative to synthetic fibers in designing load-bearing structural honeycombs, limiting the overall CO_2 emissions of engineering structures.

Acknowledgments

The authors acknowledge the China Scholarship Council (CSC No. 202106630029) for their financial support. In addition, they thank the technicians from the Delft Aerospace Structures and Materials Laboratory for their technical support.

Author contributions

Li Qian-qian: Writing - original draft, Visualization, Investigation. Yasmine Mosleh: Writing - review & editing, Supervision. Zhang Hong-hua: Investigation, Data curation. Li Wei: Writing – review & editing, Supervision. R.C. Alderliesten: Writing – review & editing, Supervision.

Declaration of conflicting interests

The author(s) declared no potential conflicts of interest with respect to the research, authorship, and/or publication of this article.

Funding

The author(s) disclosed receipt of the following financial support for the research, authorship, and/or publication of this article: this work was supported by the China Scholarship Council (CSC No. 202106630029).

ORCID iDs

Qian-qian Li https://orcid.org/0000-0001-9580-931X
Yasmine Mosleh https://orcid.org/0000-0002-7322-1539
Wei Li https://orcid.org/0000-0002-1561-166X

Data availability statement

Data will be made available on request.

Supplemental Material

Supplemental material for this article is available online.

References

1. Wu HX, Liu Y and Zhang XC. In-plane crushing behavior and energy absorption design of composite honeycombs. *Acta Mech Sin* 2018; 34(6): 1108–1123.
2. Tan XC and Chen XG. Parameters affecting energy absorption and deformation in textile composite cellular structures. *Mater Des* 2005; 26(5): 424–438.
3. Chen DH. Bending deformation of honeycomb consisting of regular hexagonal cells. *Compos Struct* 2011; 93(2): 736–746.

4. Stocchi A, Colabella L, Cisilino A, et al. Manufacturing and testing of a sandwich panel honeycomb core reinforced with natural-fiber fabrics. *Mater Des* 2014; 55: 394–403.
5. Vitale JP, Francucci G, Xiong J, et al. Failure mode maps of natural and synthetic fiber reinforced composite sandwich panels. *Compos Appl Sci Manuf* 2017; 94: 217–225.
6. Song SJ, Xiong C, Yin JH, et al. Fabrication and mechanical behavior of an all-composite interlocked triangular honeycomb sandwich structure: experimental investigation and numerical analysis. *Polym Compos* 2022; 44(2): 833–849.
7. Andrew JJ, Alhashmi H, Schiffer A, et al. Energy absorption and self-sensing performance of 3D printed CF/PEEK cellular composites. *Mater Des* 2021; 208: 109863.
8. Wei XY, Xiong J, Wang J, et al. New advances in fiber-reinforced composite honeycomb materials. *Sci China Technol Sci* 2020; 63(8): 1348–1370.
9. Antony S, Cherouatl A and Montay G. Hemp fibre woven fabrics / polypropylene based honeycomb sandwich structure for aerospace applications. *Adv Aircr Spacecr Sc* 2019; 6(2): 87–103.
10. Pehlivan L and Baykasoğlu C. An experimental study on the compressive response of CFRP honeycombs with various cell configurations. *Compos B Eng* 2019; 162: 653–661.
11. Wei XY, Li DF and Xiong J. Fabrication and mechanical behaviors of an all-composite sandwich structure with a hexagon honeycomb core based on the tailor-folding approach. *Compos Sci Technol* 2019; 184: 107878.
12. Wei XY, Wu QQ, Gao Y, et al. Composite honeycomb sandwich columns under in-plane compression: optimal geometrical design and three-dimensional failure mechanism maps. *Eur J Mech Solid* 2022; 91: 104415.
13. Wei X, Wu Q, Gao Y, et al. Bending characteristics of all-composite hexagon honeycomb sandwich beams: experimental tests and a three-dimensional failure mechanism map. *Mech Mater* 2020; 148: 103401.
14. Gu QJ, Quan ZZ, Yu JY, et al. Structural modeling and mechanical characterizing of three-dimensional four-step braided composites: a review. *Compos Struct* 2019; 207: 119–128.
15. Bilisik K. Three-dimensional braiding for composites: a review. *Textil Res J* 2012; 83(13): 1414–1436.
16. Li QQ, Zhang HH, Mosleh Y, et al. Development and analysis of a three-dimensional braided honeycomb structure. *Textil Res J* 2022; 93(9-10): 2078–2094.
17. Habib FN, Iovenitti P, Masood SH, et al. Cell geometry effect on in-plane energy absorption of periodic honeycomb structures. *Int J Adv Manuf Technol* 2017; 94(5-8): 2369–2380.
18. Jin T, Zhou ZW, Liu ZG, et al. Size effects on the in-plane mechanical behavior of hexagonal honeycombs. *Sci Eng Compos Mater* 2016; 23(3): 301–307.
19. Li QQ, Mosleh Y, Alderliesten RC, et al. Effects of different joint wall lengths on in-plane compression properties of 3D braided jute/epoxy composite honeycombs. *J Reinforc Plast Compos* 2023; 93(9-10): 2078–2094.
20. Khan MK, Baig T and Mirza S. Experimental investigation of in-plane and out-of-plane crushing of aluminum honeycomb. *Mater Sci Eng* 2012; 539: 135–142.
21. Dai XJ, Ye HY, Yang W, et al. Mechanical behaviors of inner and outer sidewalls of honeycomb cores subjected to out-of-plane compression. *Aero Sci Technol* 2022; 127: 107659.
22. Sun DQ. Out-of-Plane quasi-static compression of aluminum hexagonal honeycomb cores - a finite element analysis. *Adv Mater Res* 2011; 368-373: 339–343.
23. Zhai JY, Zhang DG, Li M, et al. Out-of-plane energy absorption and crush behavior of origami honeycomb. *Thin-Walled Struct* 2022; 181: 109966.
24. Iftimiciuc M, Derluyn A, Pflug J, et al. Out-of-plane compression mechanism of a novel hierarchical sandwich honeycomb core. *J Sandwich Struct Mat* 2023; 25(5): 518–536.
25. Li WP, Qiu C, Li ZS, et al. A failure criterion for honeycomb structures considering the onset of instability under out-of-plane loads. *J Sandwich Struct Mat* 2020; 23(8): 3519–3539.
26. Zhai JY, Liu YF, Geng XY, et al. Energy absorption of pre-folded honeycomb under in-plane dynamic loading. *Thin-Walled Struct* 2019; 145: 106356.
27. Thomas T and Tiwari G. Energy absorption and in-plane crushing behavior of aluminium reinforced honeycomb. *Vacuum* 2019; 166: 364–369.
28. Jute Yarn [Z]. https://item.m.jd.com/product/16668655717.html?&utm_source=iosapp&utm_medium=appshare&utm_campaign=t_335139774&utm_term=CopyURL&ad_od=share&gx=RnEykmANaGbfztRP–txXThAd-R6vdkwudvu.
29. Epoxy. https://www.hexion.com/en-US/our-products/.
30. Epoxy. https://www.swancor.com.cn/product_detail.aspx?cid=133&id=173.
31. Hao WF, Yuan YN, Yao XF, et al. Computational analysis of fatigue behavior of 3D 4-directional braided composites based on unit cell approach. *Adv Eng Software* 2015; 82: 38–52.
32. Chen L, Tao XM and Choy CL. RETRACTED: on the microstructure of three-dimensional braided preforms. *Compos Sci Technol* 1999; 59(3): 391–404.
33. Alkhader M, Iyer S, Shi W, et al. Low frequency acoustic characteristics of periodic honeycomb cellular cores: the effect of relative density and strain fields. *Compos Struct* 2015; 133: 77–84.
34. Chen JY, Fang H, Liu WQ, et al. Energy absorption of foam-filled multi-cell composite panels under quasi-static compression. *Compos B Eng* 2018; 153: 295–305.
35. Papka SD and Kyriakides S. In-plane crushing of a polycarbonate honeycomb. *Int J Solid Struct* 1998; 35(3-4): 239–267.
36. Scott DP and Stelios K. In-plane compressive response and crushing of honeycomb. *J Mech Phys Solid* 1994; 42(10): 1499–1532.